

Radical Cations of Phenoxazine and Dihydrophenazine Photoredox Catalysts and Their Role as Deactivators in Organocatalyzed Atom Transfer Radical Polymerization

Daniel A. Corbin, Blaine G. McCarthy, Zach van de Lindt, and Garret M. Miyake*



Cite This: *Macromolecules* 2021, 54, 4726–4738



Read Online

ACCESS |



Metrics & More

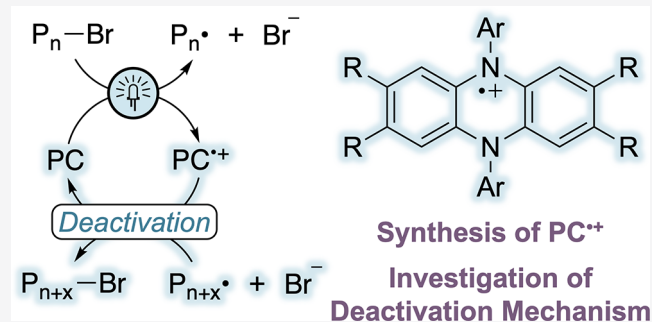


Article Recommendations



Supporting Information

ABSTRACT: Radical cations of photoredox catalysts used in organocatalyzed atom transfer radical polymerization (O-ATRP) have been synthesized and investigated to gain insight into deactivation in O-ATRP. The stability and reactivity of these compounds were studied in two solvents, *N,N*-dimethylacetamide and ethyl acetate, to identify possible side reactions in O-ATRP and to investigate the ability of these radical cations to deactivate alkyl radicals. A number of other factors that could influence deactivation in O-ATRP were also probed, such as ion pairing with the radical cations, radical cation oxidation potential, and halide oxidation potential. Ultimately, these studies enabled radical cations to be employed as reagents during O-ATRP to demonstrate improvements in polymerization control with increasing radical cation concentrations. In the polymerization of acrylates, this approach enabled superior molecular weight control, a decrease in polymer dispersity from 1.90 to 1.44, and an increase in initiator efficiency from 78 to 102%. This work highlights the importance of understanding the mechanism and side reactions of O-ATRP, as well as the importance of catalyst radical cations for successful O-ATRP.



INTRODUCTION

The development of polymerization methods that exhibit precise control over polymer molecular weight, dispersity (\bar{D}), and structure has long been a focus of polymer chemistry.^{1–4} Early examples of controlled polymerizations, also referred to as “living” polymerizations, were technically challenging to execute and required demanding reaction conditions,⁵ limiting their broad utility. However, with the advent of controlled radical polymerization (CRP) methods,^{6–9} precision polymer synthesis has become more powerful and accessible. One recently developed CRP is organocatalyzed atom transfer radical polymerization (O-ATRP), which employs organic photoredox catalysts (PCs) to synthesize well-defined polymers under mild, metal-free conditions.^{10,11}

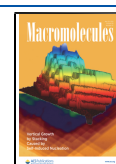
Similar to traditional atom transfer radical polymerization (ATRP) methods,^{12–14} O-ATRP controls polymer growth through a reversible deactivation mechanism (Figure 1a). During this process, the PC activates a “dormant” polymer possessing a terminal C–Br bond by reduction of the polymer chain end, generating a carbon-centered radical capable of propagation as well as Br[–] and the PC radical cation (PC^{•+}). As with all radical polymerizations, the propagating radical is susceptible to irreversible termination by reaction with other radicals in solution. As such, a key feature of O-ATRP is reversible deactivation, wherein the PC^{•+} mediates reinstallation of Br on the polymer chain end to lower the

concentration of radicals in solution. Macroscopically, this process minimizes irreversible termination reactions while allowing the polymer chain to be reactivated for subsequent chain growth, enabling control over the polymer structure.

While O-ATRP retains many of the advantages of traditional ATRP as well as some added benefits, such as mild and metal-free reaction conditions, it remains relatively limited in monomer scope and mechanistic understanding. Previously, limitations in monomer scope have generally been addressed through the development of new catalysts. For example, Matyjaszewski extended the scope of O-ATRP from methacrylates to acrylonitrile by developing new phenothiazine catalysts,¹⁵ although phenyl phenothiazine, first reported by Hawker for the O-ATRP of methacrylates,¹¹ exhibited the best performance.¹⁵ The development of dihydrophenazine¹⁶ and phenoxazine¹⁷ catalysts ultimately led to the controlled polymerization of vinylcyclopropanes with tunable polymer backbone composition.¹⁸ Through further development of the dihydrophenazine family, the controlled polymerizations of

Received: March 23, 2021

Published: May 3, 2021



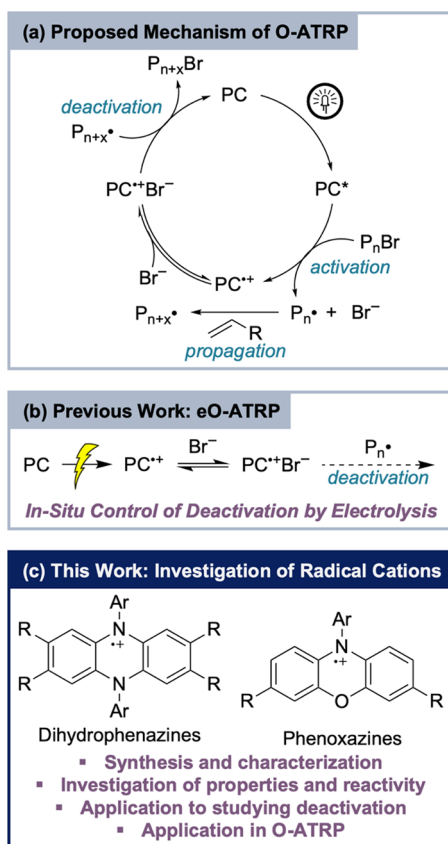


Figure 1. Proposed mechanism of O-ATRP (a) and previous work to improve deactivation during O-ATRP (b). This work (c) aims to develop a better understanding of deactivation, the species involved in this step, and how they can be used to improve polymerization control in O-ATRP.

styrene¹⁹ and various acrylates²⁰ were achieved. Finally, the first example of the controlled polymerization of acrylate monomers via O-ATRP came through the introduction of dihydroacridine catalysts in 2020, which feature strongly oxidizing radical cations [$E^\circ(PC^{\bullet+}/PC)$] capable of controlling the fast propagation of acrylates through deactivation.²¹

In an alternative approach, we recently reported the first application of electrolysis in O-ATRP in an attempt to gain external control of deactivation during a polymerization.²² We reasoned that applying an oxidizing electrochemical potential to a polymerization solution would increase the concentration of the PC radical cation ($PC^{\bullet+}$), which would, in turn, lead to improved deactivation and polymerization control during O-ATRP (Figure 1b). While this hypothesis was ultimately supported, this work highlighted limitations in our understanding of the mechanism of this method, and it inspired new questions to guide future experimentation, namely, is $PC^{\bullet+}$ the deactivator in O-ATRP, does $PC^{\bullet+}$ engage in side reactions that inhibit deactivation, and what factors influence the ability of a $PC^{\bullet+}$ to effectively mediate deactivation?²² In other words, this work highlighted the necessity of furthering our mechanistic understanding of O-ATRP.

Although several investigations of the O-ATRP mechanism have been previously reported, the majority of these reports focus on activation^{23–26} and the impact of PC photophysics on this step.^{27–29} With regard to deactivation, only a handful of reports exist,^{26,30} despite this step being critical to polymerization control. Further, these investigations relied

primarily on computational methods rather than experimental evidence to probe the mechanism of deactivation²⁶ and impact of ion pairing³⁰ in this process. While the results of these studies were certainly informative and served as useful guides for future development, experimental investigation of the deactivation process and methods to manipulate this process are still needed.

In the present work (Figure 1c), we attempt to address these limits in our understanding of deactivation in O-ATRP through the investigation of PC radical cations—the key catalytic species we propose mediate this process. To do so, several radical cations of O-ATRP PCs are synthesized and characterized for the first time. Through investigation of the reactivity of these compounds, new side reactions are identified that can inhibit deactivation in O-ATRP. Further, through the development of a deactivation model reaction, evidence is found supporting the role of $PC^{\bullet+}Br^-$ as the deactivator, and factors influencing this process are identified. The most notable factors include the radical cation oxidation potential [$E^\circ(PC^{\bullet+}/PC)$] and the oxidation potential of the halide [$E^\circ(X^\bullet/X^-)$], both of which can directly impact the rate of deactivation. By investigating ion pairing with $PC^{\bullet+}$, it is found that the choice of reaction solvent is far more influential than $PC^{\bullet+}$ structure for the formation of a $PC^{\bullet+}$ ion pair. Finally, by employing an isolated radical cation in O-ATRP, it is demonstrated that these compounds can be used to improve polymerization control, further supporting their role in deactivation. Altogether, this work highlights the utility of PC radical cations in O-ATRP, as well as the importance of mechanistic understanding for the continued development of O-ATRP.

RESULTS AND DISCUSSION

Synthesis and Characterization of Radical Cations.

Synthesis. Radical cations of 1–11 (Figure 2a) were synthesized using nitrosonium hexafluorophosphate, as the oxidation potential of NO^+ is more than sufficient to oxidize 1–11 [$E^\circ(NO^+/NO) = 1.25$ V,³¹ $E_{1/2} \sim E^\circ(PC^{\bullet+}/PC) = 0.14–0.73$ V, both vs saturated calomel electrode (SCE) in MeCN]. Since the byproduct of this reaction is $NO(g)$, the product can be easily isolated by precipitation and washing with hexanes. For PCs 1–5, it should be noted that the cyclic voltammograms in MeCN exhibit two reversible oxidations that could be accessible using $NOPF_6$ (see Section S3 of the Supporting Information). As such, precise stoichiometry is necessary to avoid overoxidation of these compounds to the dicationic species. For crystallography, crystal growth was attempted using various methods with a range of $PC^{\bullet+}PF_6^-$ salts. However, crystals of these compounds suitable for single-crystal X-ray diffraction (SCXRD) could not be obtained. Given the large size of the radical cations, we envisioned that the PF_6^- anion might be too small to enable effective crystal packing and that a larger counterion might be beneficial. As such, radical cations for SCXRD analysis were synthesized using tris(4-bromophenyl)ammonium hexachloroantimonate, yielding $4^{\bullet+}SbCl_6^-$ and $9^{\bullet+}SbCl_6^-$. In both cases, crystallization by vapor diffusion (see Section S2 of the Supporting Information for details) gave needles of suitable quality for X-ray diffraction studies.

Spectroscopic Characterization. To verify the identity of each $PC^{\bullet+}$, absorption spectra of the isolated compounds were compared to $PC^{\bullet+}$ spectra obtained using spectro-electrochemistry (Figure 2b). The spectra of the isolated compounds

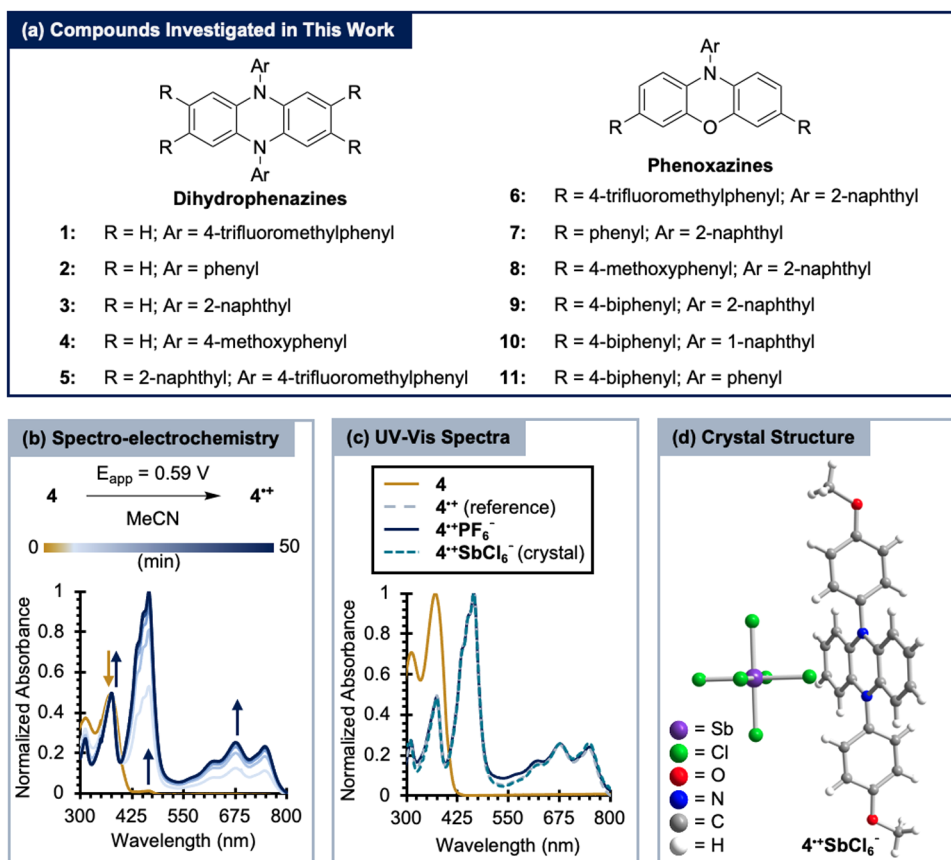


Figure 2. (a) Structures of photoredox catalysts studied in this work. (b) Representative example of radical cation spectra obtained by spectro-electrochemistry in acetonitrile. (c) Representative comparison of UV-vis spectra for a PC (solid, yellow), the PC^{•+} obtained by spectro-electrochemistry (dashed, light blue), PC^{•+}PF₆[−] (solid, dark blue), and a redissolved PC^{•+}SbCl₆[−] crystal (dashed, teal). (d) Crystal structure of a phenazine radical cation (solvent molecule is removed for clarity).

were found to agree well with the reference spectra (Figure 2c), supporting the successful synthesis of each PC^{•+}. In addition, the spectra of 4^{•+}PF₆[−] and 4^{•+}SbCl₆[−] were nearly identical, suggesting that the identity of the counteranion has a negligible impact on the spectroscopic properties of the radical cation.

Since crystals of 4^{•+}SbCl₆[−] and 9^{•+}SbCl₆[−] were obtained and analyzed by SCXRD to determine their crystal structures (see the Crystallography section), we wondered if the solid-state spectra of these compounds would match their solution spectra. Unfortunately, the crystals obtained were insufficiently transparent to obtain well-resolved absorption spectra in the solid state, so this comparison could not be made. Instead, the crystals were redissolved in MeCN and their spectra were measured in solution (Figure 2c). The agreement of these spectra and the PC^{•+}PF₆[−] spectra further support the identity of the PC^{•+} salts.

Electrochemical Characterization. For each of the radical cations synthesized, estimates of their purities were obtained by the measurement of their open-circuit potentials (E_{ocp}) in MeCN. According to the Nernst equation (eq 1), the E_{ocp} of a PC^{•+} solution is dependent on the $E_{1/2}$ of the redox couple and the relative quantities of PC and PC^{•+}

$$E_{\text{ocp}} = E_{1/2} + \frac{RT}{F} \ln \left(\frac{[\text{PC}^{\bullet+}]}{[\text{PC}]} \right) \quad (1)$$

where R is the ideal gas constant, T is the absolute temperature, and F is Faraday's constant. Rearranging this

equation, an expression giving the ratio of PC^{•+} to PC based on the E_{ocp} and $E_{1/2}$ can be written (eq 2). Using eq 2, the purity of each PC^{•+}PF₆[−] salt was estimated to be ~97% or greater. To verify the accuracy of this method, elemental analysis was also performed for 11^{•+}PF₆[−], which agreed well with the calculated elemental composition of this compound (see the Supporting Information)

$$\frac{[\text{PC}^{\bullet+}]}{[\text{PC}]} = e^{F(E_{\text{ocp}} - E_{1/2})/RT} \quad (2)$$

Crystallography. Single-crystal X-ray diffractometry was performed using crystals obtained for 4^{•+}SbCl₆[−] (Figure 2d) and 9^{•+}SbCl₆[−]. In each case, the SbCl₆[−] anion was found centered above the aromatic core of the PC^{•+} and the PC^{•+} was found to cocrystallize with 1 equiv of the solvent molecule (Figures S54 and S55). While 4^{•+}SbCl₆[−] exhibited minimal disorder and was easily refined, 9^{•+}SbCl₆[−] exhibited significant disorder that had to be modeled during refinement, namely, the 2-naphthyl ring at the *N*-aryl position was disordered over two positions, presumably because the substituent can rotate about the C–N bond. In both cases, the refined crystal structures matched the structures anticipated for the radical cations. Combined with the spectroscopic data presented above, these data provide further support for the identities of these PC^{•+} salts.

Stability of Radical Cations in Solution. During initial work with these compounds, it was noticed that the stability of PC^{•+} in solution was strongly dependent on the solvent. To

understand the factors influencing the stability of $\text{PC}^{\bullet+}$, a series of experiments were performed to follow the decomposition of $\text{PC}^{\bullet+}$ using UV–vis spectroscopy in solvents relevant to O-ATRP. Since it was previously observed that dihydrophenazine PCs can undergo side reactions to be substituted at the PC core,²⁰ $5^{\bullet+}$ was primarily used for these investigations as its core positions are protected by 2-naphthyl substituents.

In *N,N*-dimethylacetamide (DMAc), decomposition of $5^{\bullet+}$ was observed with and without irradiation (Figure 3).

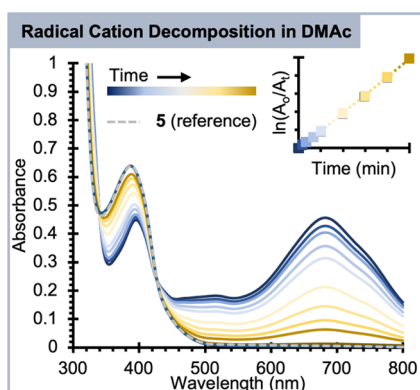


Figure 3. Representative example of UV–vis spectra following the disappearance of $5^{\bullet+}$ in DMAc under irradiation with a white light-emitting diode (LED). The inset shows linear pseudo-first-order kinetics following the absorption at the $\lambda_{\text{max}} = 682$ nm.

Following the kinetics of these reactions by UV–vis revealed that the decomposition reaction is accelerated by irradiation with white light (Figures S56 and S58) and exhibits pseudo-first-order kinetics in the dark ($k_{\text{obs}} = 0.00064 \text{ M}^{-1} \text{ s}^{-1}$) and under irradiation ($k_{\text{obs}} = 0.39 \text{ M}^{-1} \text{ s}^{-1}$). The observed increase in the rate of $5^{\bullet+}$ disappearance with light suggests the possibility of excited-state reactivity, which has previously been observed for similar radical cations with electron-rich substrates tethered at the *N*-aryl position.³² By contrast, $5^{\bullet+}$ exhibited excellent stability in ethyl acetate (EtAc) regardless of irradiation (Figures S65 and S67).

To investigate whether this behavior is unique to $5^{\bullet+}$, the same study was performed with a noncore-substituted phenazine ($3^{\bullet+}$; Figures S59 and S61) and a phenoxazine

radical cation ($10^{\bullet+}$; Figures S62 and S64). The same behavior was found but with a greater rate for the disappearance of $10^{\bullet+}$ relative to $5^{\bullet+}$ and $3^{\bullet+}$. As $10^{\bullet+}$ is significantly more oxidizing in the ground state [$E_{1/2} \sim E^\circ(10^{\bullet+}/10) = 0.66 \text{ V}$ vs SCE in MeCN], its greater reactivity may be due to its stronger oxidation potential.

In every case, an isosbestic point was observed during the disappearance of $\text{PC}^{\bullet+}$, indicating conversion to a single product. Further, when the reaction was carried out to high conversion (as indicated by complete loss of the $\text{PC}^{\bullet+}$ signal), the product spectrum closely resembled that of the PC. These data, combined with the observation of pseudo-first-order kinetics, led us to hypothesize that decomposition of $\text{PC}^{\bullet+}$ occurs by single electron transfer from DMAc to generate the neutral PC. Under irradiation, this reaction might proceed through a more oxidizing $\text{PC}^{\bullet+}$ excited state, which would explain why the rate of the reaction increases. However, this possibility will be discussed further in a later section (see the Investigation of Radical Cation Side Reactions section).

While the oxidation of DMAc by $\text{PC}^{\bullet+}$ is consistent with the data presented above, it is surprising given that the oxidation potential of DMAc [$E^\circ_{\text{calc}}(\text{DMAc}^+/\text{DMAc}) = 1.98 \text{ V}$ vs SCE] is significantly more positive than that of any $\text{PC}^{\bullet+}$ in this work [$E_{1/2} \sim E^\circ(\text{PC}^{\bullet+}/\text{PC}) = 0.14\text{--}0.73 \text{ V}$ vs SCE]. To probe this reaction further, a kinetic isotope study was performed using DMF and deuterated dimethylformamide (*d*₇-DMF), assuming similar reactivity would be observed as with DMAc (see the Section S4 in the Supporting Information). A normal kinetic isotope effect was observed in the dark ($k_{\text{H}}/k_{\text{D}} = 5.9$), and an inverse isotope effect was observed under irradiation ($k_{\text{H}}/k_{\text{D}} = 0.18 \pm 0.04$). As inverse equilibrium isotope effects are more common than inverse kinetic isotope effects,³³ this result led us to believe that an equilibrium might be involved in the excited-state oxidation of DMAc and DMF. We hypothesize that $\text{PC}^{\bullet+}$ preassociates with a solvent molecule prior to photoinduced electron transfer. However, regardless of the mechanism of this reaction, the observation of this isotope effect supports a direct reaction between DMF and $5^{\bullet+}$.

Several alternative hypotheses explaining the decomposition of $5^{\bullet+}$ were also investigated, including the oxidation of the PF_6^- anion and the possibility of solvent impurities. To rule out a reaction with PF_6^- , a solution of $5^{\bullet+}\text{PF}_6^-$ was prepared

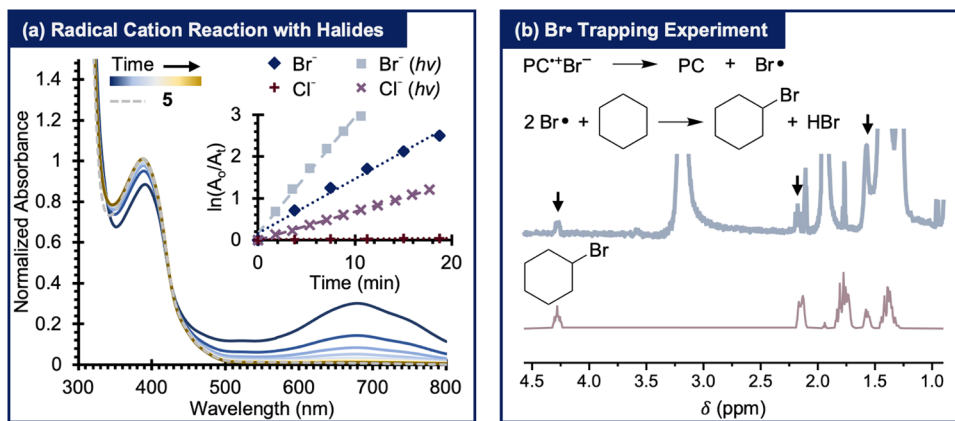


Figure 4. (a) Representative example of UV–vis spectra following the disappearance of $5^{\bullet+}$ in the presence of LiBr. The inset shows a comparison of pseudo-first-order kinetics demonstrating the impact of irradiation and the halide identity. (b) Identification by ^1H NMR of bromocyclohexane formed from Br^\bullet after oxidation of Br^- by $5^{\bullet+}$.

in deuterated DMF and irradiated with white LEDs. After the solution turned from dark blue to yellow, indicating conversion of $\mathbf{5}^{\bullet+}$ to $\mathbf{5}$, the reaction products were analyzed by ^{19}F NMR (Figure S68). The resulting spectrum was consistent with the preservation of the PF_6^- anion. To test for solvent impurities, DMF and d_7 -DMF were analyzed by gas chromatography (Figures S70 and S71). Neither analysis revealed volatile impurities that could account for the observed reactivity, supporting a direct reaction between $\mathbf{5}^{\bullet+}$ and DMF.

Investigation of Radical Cation Side Reactions.

Impact of Irradiation on Radical Cation Reactivity. To further investigate possible reactivity from the excited state of $\mathbf{5}^{\bullet+}$, a series of reactions were performed in the presence of substrates with increasing oxidation potentials. For substrates with lower oxidation potentials [$E^\circ(\text{S}^+/ \text{S}) \leq 1$ V vs SCE], the slow disappearance of $\mathbf{5}^{\bullet+}$ was observed with equal kinetics under irradiation and in the dark (Table S6). Since irradiation did not impact this reaction, a ground-state mechanism is proposed to be most likely with these substrates. Instead, for substrates with greater oxidation potentials, no reactivity was observed either in the dark or under irradiation, with DMAc being the only exception at high concentrations. This observation may be linked to the excited-state lifetime of $\mathbf{5}^{\bullet+}$, which could be too short to engage in bimolecular reactions in solution unless the substrate is present in high enough concentration (i.e., solvent quantities) to overcome the lifetime of this species.

In the Presence of Bromide. The reactivity of $\mathbf{5}^{\bullet+}$ was also investigated in the presence of halides (Figure 4a), given the relevance of these ions to O-ATRP. Although some experiments were performed in ethyl acetate (Figures S104 and S106), the reaction of $\mathbf{5}^{\bullet+}$ with halides proved challenging to track due to the rate of the reaction. As such, DMAc was used instead for these investigations.

In the presence of 0.1 M LiBr in the dark, $\mathbf{5}^{\bullet+}$ exhibited reactivity ($k_{\text{Br-dark}} = 0.14 \pm 0.02 \text{ M}^{-1} \text{ s}^{-1}$) that was distinguishable from the background reaction with DMAc ($k_{\text{DMAc-dark}} = 0.00064 \text{ M}^{-1} \text{ s}^{-1}$), suggesting a possible ground-state reaction between $\mathbf{5}^{\bullet+}$ and Br^- . An increase in the rate of disappearance for $\mathbf{5}^{\bullet+}$ was observed under irradiation ($k_{\text{Br-light}} = 0.31 \pm 0.06 \text{ M}^{-1} \text{ s}^{-1}$), although it is difficult to distinguish whether this change in rate was due to a reaction with Br^- or simply with DMAc ($k_{\text{DMAc-light}} = 0.39 \text{ M}^{-1} \text{ s}^{-1}$). Regardless of irradiation, the formation of $\mathbf{5}$ was observed by UV-vis in each case (Figures S100 and S102), suggesting a single electron transfer mechanism between $\mathbf{5}^{\bullet+}$ and Br^- .

Since such a reaction would be expected to generate bromine radical (Br^\bullet), an experiment was devised to probe for the presence of Br^\bullet in this reaction. To do so, the radical halogenation of alkanes was employed, wherein a halogen radical performs hydrogen atom abstraction from an alkane to generate an alkyl radical, followed by radical coupling of the alkyl radical with another halogen radical to give the halogenated alkane. The reaction of $\mathbf{5}^{\bullet+}$ and Br^- was performed in the presence of cyclohexane and monitored by ^1H NMR for the formation of bromocyclohexane. Excitingly, a small quantity of bromocyclohexane was observed (Figure 4b), supporting the hypothesized oxidation of Br^- by $\mathbf{5}^{\bullet+}$.

Finally, the kinetics of this reaction were investigated with two other radical cations. When the reaction of $\mathbf{3}^{\bullet+}$ and Br^- was followed, similar results were observed as with $\mathbf{5}^{\bullet+}$, although at a reduced rate ($k_{\text{3-dark}} = 0.02 \text{ M}^{-1} \text{ s}^{-1}$, $k_{\text{3-light}} =$

$0.08 \text{ M}^{-1} \text{ s}^{-1}$). Instead, the reaction between $\mathbf{10}^{\bullet+}$ and Br^- was too rapid to follow by UV-vis (Figure S110), even in the absence of light. These results broadly correlate with the oxidation potentials of these compounds [$E_{1/2}(\mathbf{3}^{\bullet+}/\mathbf{3}) = 0.18$ V; $E_{1/2}(\mathbf{5}^{\bullet+}/\mathbf{5}) = 0.32$ V; $E_{1/2}(\mathbf{10}^{\bullet+}/\mathbf{10}) = 0.66$ V, all vs SCE in MeCN], possibly yielding insight into their capabilities as deactivators in O-ATRP. This possibility will be discussed in greater detail later in the text (see the **Factors Influencing the Deactivation of Alkyl Radicals** section).

In the Presence of Chloride. While metal-catalyzed ATRP is often performed in the presence of bromide and chloride (either by using alkyl bromide or chloride initiators, or through the addition of halide salts),¹² O-ATRP in the presence of chloride has remained challenging. One difference between these halides is that alkyl chloride bond strengths are typically greater than alkyl bromides, which would make activation more challenging with alkyl chlorides. However, previous investigations by Matyjaszewski and co-workers have suggested that the issue with chloride may be ineffective deactivation,²⁶ though the origin of this issue remains a mystery. To investigate this limitation of O-ATRP further, the reactivity of $\mathbf{5}^{\bullet+}$ was studied in the presence of LiCl. Unlike the reaction with Br^- , that with Cl^- in the dark exhibited only a minor increase in the rate of disappearance of $\mathbf{5}^{\bullet+}$ ($k_{\text{Cl-dark}} = 0.0020 \pm 0.0007 \text{ M}^{-1} \text{ s}^{-1}$) relative to the background reaction in DMAc ($k_{\text{DMAc-dark}} = 0.00064 \text{ M}^{-1} \text{ s}^{-1}$). Irradiation with white LEDs again increased the rate of $\mathbf{5}^{\bullet+}$ disappearance ($k_{\text{Cl-light}} = 0.074 \pm 0.013 \text{ M}^{-1} \text{ s}^{-1}$), though this reaction was still slower than with Br^- both in the dark ($k_{\text{Br-dark}} = 0.14 \pm 0.02 \text{ M}^{-1} \text{ s}^{-1}$) and under irradiation ($k_{\text{Br-light}} = 0.31 \pm 0.06 \text{ M}^{-1} \text{ s}^{-1}$).

Under both irradiation conditions, the oxidation of Cl^- appears to be significantly slower than the oxidation of Br^- . This observation is consistent with the oxidation potentials of these ions [$E^\circ(\text{Br}_3^-/\text{Br}^-) = 0.7$ V, $E^\circ(\text{Cl}_3^-/\text{Cl}^-) = 1.1$ V, both vs SCE in MeCN³⁴]. As such, a possible explanation for poor deactivation in O-ATRP using Cl^- could be that it is more challenging to oxidize this ion, which leads to an overall slower rate of deactivation with Cl^- relative to Br^- . This hypothesis is further supported by experiments measuring the rate of deactivation in the presence of Br^- vs Cl^- , although these data will be discussed later (see the **Factors Influencing the Deactivation of Alkyl Radicals** section).

Despite the kinetic differences observed between Cl^- and Br^- , irradiation of $\mathbf{5}^{\bullet+}$ in the presence of Cl^- again led to the recovery of the ground-state UV-vis spectrum of $\mathbf{5}$ (Figure S115), indicating a similar redox mechanism leading to the formation of $\mathbf{5}$ and Cl^\bullet . A trapping experiment was attempted to provide evidence for the formation of Cl^\bullet , but this experiment was unsuccessful. While this result does not rule out the formation of Cl^\bullet , it further highlights the inefficiency of Cl^- oxidation by $\mathbf{5}^{\bullet+}$.

Proposed Mechanism of Substrate Oxidation. Considering the reactivity studies discussed thus far, we propose the following mechanisms for substrate oxidation by $\text{PC}^{\bullet+}$. In the ground state, substrate oxidation appears to proceed through a bimolecular electron transfer reaction, which results in the formation of neutral $\mathbf{5}$ and the oxidized substrate. Instead, in the excited state, association of the substrate with $\mathbf{5}^{\bullet+}$ prior to photoexcitation may facilitate electron transfer (Figure 5). After preassociation, irradiation of $\mathbf{5}^{\bullet+}$ could lead to photoinduced electron transfer, which is likely followed by dissociation of the product complex to yield free $\mathbf{5}$ and

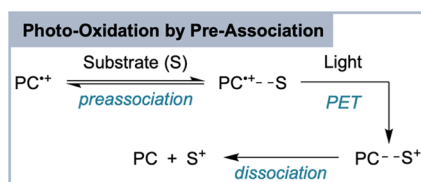


Figure 5. One proposed mechanism for substrate oxidation by photoexcited PC^{**} facilitated by preassociation of the PC^{**} and substrate.

oxidized substrate. While such an association with S^{**} is not surprising for Cl^- or Br^- , it is perhaps less anticipated for a neutral substrate such as DMAc. However, DMAc contains a lone pair of electrons at the nitrogen position as well as significant electron density around the carbonyl oxygen, which might be susceptible to a weak interaction with the positively charged PC^{**} . While this weak interaction might be negligible at low concentrations, higher concentrations may enable a small degree of association between DMAc and S^{**} , enabling excited-state reactivity. Alternatively, a bimolecular reaction between the excited state of S^{**} and the substrate may also be feasible, depending on the lifetime of this excited state and the concentration of the substrate in solution. However, deeper investigation of the photophysical properties of these radical cations is necessary to probe this possible reactivity further.

Factors Influencing the Deactivation of Alkyl Radicals. *Deactivation of Alkyl Radicals.* To better understand these radical cations in the context of deactivation, their reactions with alkyl radicals were investigated. A reaction to model deactivation in O-ATRP was devised using S^{**} in the presence of Br^- to deactivate thermally generated radicals from azobisisobutyronitrile (AIBN) (Figure 7a). To first determine whether S^{**} could operate as a radical deactivator, the formation of the brominated deactivation product was monitored by 1H NMR (Figures S118 and S119). The NMR spectrum of the model reaction showed a peak matching the expected chemical shift of the deactivation product ($\delta = 2.07$ ppm in CD_3CN), suggesting S^{**} can indeed deactivate alkyl radicals.

Previous computational investigations have attempted to determine the mechanism of deactivation using density functional theory and Marcus theory to predict the rate of deactivation via various mechanisms.²⁶ This work concluded that a termolecular mechanism was most favorable with phenyl phenothiazine as the catalyst.³⁵ Instead, we hypothesize that a bimolecular deactivation mechanism is operative, wherein PC^{**} and Br^- form an ion pair ($PC^{**}Br^-$) prior to reaction with the propagating radical (Figure 6; “concerted mechanism”). Based on the observed reactivity between S^{**} and Br^- , it was also envisioned that deactivation could occur through a stepwise mechanism. In this case, formation of the

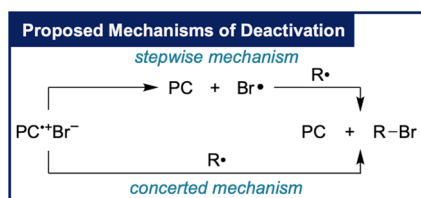


Figure 6. Hypothesized mechanisms of deactivation investigated in this work.

$PC^{**}Br^-$ ion pair might lead to the oxidation of Br^- , generating a free equivalent of Br^\bullet that could then undergo radical coupling with the radical on the polymer chain end in a subsequent step (Figure 6; “stepwise mechanism”). In either case, the products of deactivation would be the same. It should be noted that in this work, the primary catalyst family investigated was dihydrophenazines, which differ structurally from the previously investigated phenothiazines by a second *N*-aryl substituent. In addition, the radical cations of dihydrophenazines are typically much less oxidizing than those of phenothiazines. Both these properties could ultimately impact the mechanism of deactivation, leading to differences between various catalyst families.

To investigate which of these mechanisms might predominate, another model reaction employing AIBN was employed. Cyclohexane was also added to the reaction in an attempt to trap Br^\bullet during deactivation. It was reasoned that the formation of bromocyclohexane should only be observed if free Br^\bullet forms during deactivation through a stepwise mechanism. Instead, if deactivation proceeds through a concerted mechanism, a reaction between Br^\bullet and cyclohexane should be sufficiently challenging to prevent the formation of bromocyclohexane. Indeed, when this experiment was carried out using S^{**} , the primary product of the reaction was found to be that from deactivation (2-bromo-2-methylpropanenitrile), with little-to-no bromocyclohexane detectable by 1H NMR (Figures S120 and S121). This experiment suggests that a concerted mechanism may be most likely.

Bromide vs Chloride. As was discussed briefly above, O-ATRP in the presence of chloride has remained challenging, presumably due to an issue during deactivation with Cl^- .²⁶ Based on our investigations of radical cation reactivity in the presence of Br^- and Cl^- , one possible explanation for why deactivation is successful with Br^- but not Cl^- is based on their difference in oxidation potentials. Since Cl^- is more challenging to oxidize, the deactivation reaction with Cl^- is likely slower, leading to ineffective deactivation and poor polymerization control in O-ATRP.

To test this hypothesis more directly, the deactivation model reaction employed above was followed in situ using UV–vis spectroscopy (Figure 7a). By doing so, the disappearance of S^{**} during deactivation could be monitored to measure the kinetics of deactivation, yielding direct insight into factors that might influence the rate of deactivation. Unsurprisingly, when the reaction was performed in the presence of Cl^- , the disappearance of S^{**} was much slower than with Br^- (Figure 7b), indicating less efficient deactivation. In the absence of halide, the disappearance of S^{**} was only slightly slower than in the presence of Cl^- . Therefore, while deactivation still appears to occur in the presence of Cl^- , it is very slow. In O-ATRP, slow deactivation would promote a higher concentration of radicals during the reaction, ultimately increasing termination reactions and inhibiting polymerization control.

In addition to the difference in oxidation potentials of the halides, we hypothesized that the propensity of Br^\bullet and Cl^\bullet to undergo side reactions might also be important. Cl^\bullet could be more prone to H-atom abstraction than Br^\bullet based on the greater bond strength of H–Cl than H–Br,³⁶ which makes H–Cl formation more thermodynamically favorable. In turn, this greater driving force might lead to more side reactions in O-ATRP. To probe this possibility, a collector–generator

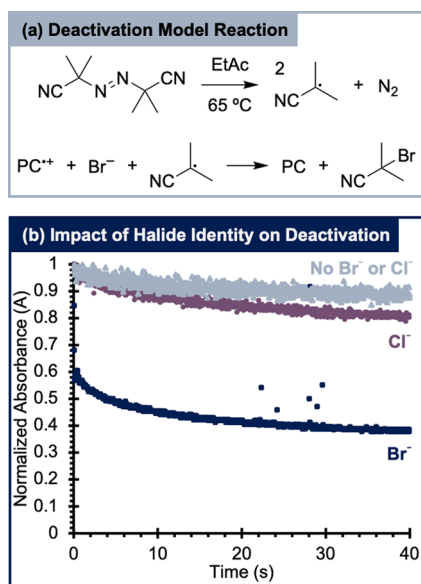


Figure 7. (a) Model reaction used in this work to investigate deactivation in O-ATRP. (b) In situ kinetics of deactivation with $5^{\bullet+}$ (monitored at 677 nm) in the presence of halides (Br^- , dark blue; Cl^- , purple) and in their absence. Data normalized to maximum absorbance at the time of $\text{PC}^{\bullet+}$ addition ($t = 0$).

experiment was performed using a rotating ring-disc electrode with LiBr or LiCl in a mixture of DMAc and methyl methacrylate (MMA) to mimic O-ATRP conditions (Figure S129). The results of these experiments revealed that 0.7% of Br^\bullet was collected, whereas 5.9% of Cl^\bullet was collected. In other words, Cl^\bullet underwent fewer side reactions than Br^\bullet . Further, if the mechanism of deactivation is in fact concerted as previous experiments suggested, the possibility of side reactions from free Br^\bullet or Cl^\bullet is likely reduced. Therefore, such side reactions may not be responsible for poor control in O-ATRP using Cl^- .

Radical Cation Structure. One long-standing hypothesis in the design of O-ATRP PCs is that increasing the oxidation potential of $\text{PC}^{\bullet+}$ increases the rate of deactivation.^{21,37} While this hypothesis has motivated the development of new PCs with strongly oxidizing radical cations,^{17,21} it has never been tested. As such, another series of model reactions was performed using $4^{\bullet+}$ [$E_{1/2}(4^{\bullet+}/4) = 0.14$ V vs SCE], $3^{\bullet+}$ [$E_{1/2}(3^{\bullet+}/3) = 0.18$ V vs SCE] and $1^{\bullet+}$ [$E_{1/2}(1^{\bullet+}/1) = 0.33$ V vs SCE], which feature increasing oxidation potentials (Figure 8). A correlation was observed between the oxidation potential of $\text{PC}^{\bullet+}$ and the rate of deactivation, supporting the validity of this hypothesis.

Since core substitution of dihydrophenazine PCs by alkyl radicals has been reported as a possible side reaction,²⁰ control experiments were performed in the absence of LiBr to rule out interference from these reactions (Figures S125 and S127). Further, this experiment was also attempted with radical cations of phenoxazines 6–8, although these reactions proceeded too rapidly to be measured quantitatively (Figure S128).

Ion Pairing in Radical Cations. Given that the $\text{PC}^{\bullet+}\text{Br}^-$ ion pair is the hypothesized deactivator in O-ATRP, the susceptibility of $\text{PC}^{\bullet+}$ to form this ion pair could be important for effective deactivation during a polymerization. To probe the variables impacting ion pairing with $\text{PC}^{\bullet+}$, the equilibrium association constants (K_{assoc}) of various $\text{PC}^{\bullet+}\text{PF}_6^-$ salts were

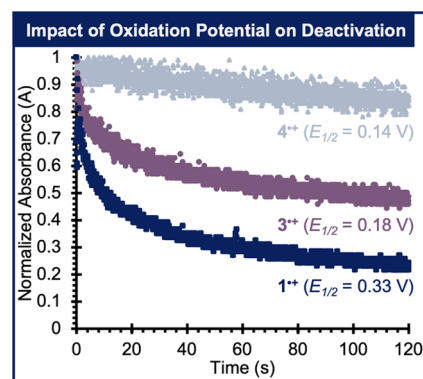


Figure 8. In situ kinetics of deactivation with three dihydrophenazine radical cations demonstrating the impact of PC oxidation potential [$E_{1/2} \sim E^\circ(\text{PC}^{\bullet+}/\text{PC})$, all in V vs SCE] on the rate of deactivation. Kinetics monitored at 682 nm ($1^{\bullet+}$), 680 nm ($3^{\bullet+}$), and 677 nm ($4^{\bullet+}$). Data normalized to the maximum absorbance at the time of $\text{PC}^{\bullet+}$ addition ($t = 0$).

measured using conductometry. While $\text{PC}^{\bullet+}\text{PF}_6^-$ is not the true deactivator in O-ATRP, we hypothesized that these salts would exhibit similar trends in ion pairing as $\text{PC}^{\bullet+}\text{Br}^-$, allowing broad conclusions to be drawn.

To understand how the radical cation structure impacts ion pairing, K_{assoc} was measured for each $\text{PC}^{\bullet+}\text{PF}_6^-$ synthesized (Table S8). To our surprise, all of the radical cations investigated showed K_{assoc} values within roughly 1 order of magnitude of each other ($\Delta\Delta G_{\text{assoc}} \sim 1$ kcal mol⁻¹), which is only slightly outside of the error of the measurement (Table S10). Coupled with the fact that no trends in the conductometry data were observed, these results suggest that the impact of $\text{PC}^{\bullet+}$ structure on ion pairing in $\text{PC}^{\bullet+}\text{PF}_6^-$ is minimal at best. By contrast, the solvent appears to have a much greater impact on ion pairing in $\text{PC}^{\bullet+}\text{PF}_6^-$. When conductometry was performed with $1^{\bullet+}\text{PF}_6^-$ in four different solvent systems, from DMAc to tetrahydrofuran (THF) (Table S9), K_{assoc} varied over several orders of magnitude (10^2 – 10^6 M⁻¹, $\Delta\Delta G_{\text{assoc}} \sim 5$ kcal mol⁻¹). Further, K_{assoc} varied predictably as a function of the solvent dielectric constant, as suggested by theory (Figure S147).³⁸ Thus, while the structure of $\text{PC}^{\bullet+}$ appears to have only a minor influence on ion pairing, the choice of the solvent can be very impactful.

Impact of Radical Cations in O-ATRP. Polymerization of Methyl Methacrylate. To better understand the role of radical cations in O-ATRP, polymerizations were conducted in the presence of increasing quantities of $\text{PC}^{\bullet+}$. In each case, the kinetics of the polymerizations and the resulting polymers were characterized to understand how the addition of $\text{PC}^{\bullet+}$ impacted the reaction. Since $\text{PC}^{\bullet+}$ is the hypothesized deactivator in O-ATRP, we anticipated that adding supplemental $\text{PC}^{\bullet+}$ to O-ATRP would result in (1) a lower observed rate of the polymerization; (2) more linear molecular weight growth; (3) lower \bar{D} ($1 < \bar{D} \leq 1.5$) throughout the polymerization, especially at low monomer conversions; and (4) improved initiator efficiency ($I^* \sim 100\%$).

For initial investigations, the polymerization of MMA using **5** under published conditions³⁹ was targeted. While DMAc has typically been the solvent of choice for O-ATRP, ethyl acetate was chosen given the greater stability of $5^{\bullet+}\text{PF}_6^-$ in ethyl acetate relative to DMAc. In addition, LiBr was added to these polymerizations ($[\text{LiBr}] = [\mathbf{5}] + [5^{\bullet+}]$) to facilitate the

Table 1. Initial Polymerization Results for the O-ATRP of MMA with Increasing Quantities of Supplemental Deactivator^a

entry	[S]:[S ^{•+}]	time (h)	conv. (%) ^b	k _{obs} (M ⁻¹ h ⁻¹) ^c	M _{n,theo} (kDa)	M _{n,exp} (kDa) ^d	\bar{D} ^d	I* (%) ^e
1 ^f	1:0	24	67.5	0.046	7.01	6.19	1.19	113
2	1:0	24	71.3	0.053	7.40	6.71	1.14	110
3	3:1	24	64.8	0.046	6.74	6.38	1.16	106
4	1:1	24	68.1	0.044	7.07	6.87	1.12	103
5	1:3	24	55.4	0.039	5.80	5.60	1.16	103
6	0:1	24	75.8	0.037	7.84	7.36	1.10	107

^aUnless stated otherwise, [MMA]/[DBMM]/[S/S^{•+}]/[LiBr] = [1000]:[10]:[0.1]:[0.1] (see Section S11 of the Supporting Information for full experimental details). ^bDetermined by ¹H NMR. ^cDetermined from the first three time points (1, 2, and 4 h). ^dDetermined by gel permeation chromatography (GPC). ^eInitiator efficiency (I*) = (M_{n,theo}/M_{n,exp}) × 100%. ^fReaction run without LiBr.

Table 2. Initial Polymerization Results for the O-ATRP of MA with Increasing Quantities of Supplemental Deactivator^a

entry	[S]:[S ^{•+}]	time (h)	conv. (%) ^b	k _{obs} (M ⁻¹ h ⁻¹) ^c	M _{n,theo} (kDa)	M _{n,exp} (kDa) ^d	\bar{D} ^d	I* (%) ^e
7 ^f	1:0	6	80.7	0.40	7.20	8.59	2.21	84
8	1:0	6	91.6	0.89	8.14	11.6	1.77	70
9	3:1	6	84.2	0.58	7.50	8.09	1.88	93
10	1:1	6	70.6	0.29	6.33	8.40	1.67	75
11	1:3	6	73.3	0.28	6.57	6.98	1.65	94
12	0:1	6	61.4	0.17	5.54	6.45	1.55	86

^aUnless stated otherwise, [MA]/[DBMM]/[S/S^{•+}]/[LiBr] = [1000]:[10]:[0.1]:[0.1] (see Section S12 of the Supporting Information for full experimental details). ^bDetermined by ¹H NMR. ^cDetermined from the first three time points (0.5, 1, and 1.5 h). ^dDetermined by GPC. ^eInitiator efficiency (I*) = (M_{n,theo}/M_{n,exp}) × 100%. ^fReaction run without LiBr.

formation of the PC^{•+}Br⁻ ion pair. Since the addition of Br⁻ salts alone has been shown to improve deactivation,²⁶ we first investigated the impact of this reagent on polymerization control (Table 1, entries 1 and 2). Unsurprisingly, adding LiBr resulted in a slight decrease in \bar{D} (\bar{D} = 1.14 with LiBr vs 1.19 without), although otherwise similar polymerization results.

To then understand the impact of adding S^{•+}PF₆⁻ to this polymerization, the ratio of [S]:[S^{•+}] was varied while maintaining the overall catalyst loading ([S] + [S^{•+}] = 100 ppm) constant (Table 1, entries 2–6) in the presence of 100 ppm LiBr. Overall, no significant improvements in polymerization control were observed upon increasing [S^{•+}] (ex. \bar{D} = 1.14 for [S]:[S^{•+}] = 1:0 vs \bar{D} = 1.10 for [S]:[S^{•+}] = 0:1), presumably because the polymerization with S already exhibits excellent polymerization control. However, a decrease in the rate of the polymerizations was observed, especially during the first several hours (k_{obs} = 0.053 M⁻¹ s⁻¹ for [S]:[S^{•+}] = 1:0 vs k_{obs} = 0.037 M⁻¹ s⁻¹ for [S]:[S^{•+}] = 0:1), consistent with improved deactivation.

For polymerizations started with only S^{•+}PF₆⁻, one might expect activation to be inaccessible due to the lack of S. However, we hypothesized that the reaction between S^{•+} and Br⁻ would generate a small quantity of S, allowing the polymerization to begin upon irradiation. Support for this hypothesis was found when control reactions were performed (Table S11), which showed significantly reduced conversion in the absence of LiBr (8.3 vs 75.8%). Further, visual inspection of this polymerization revealed that the reaction remained dark blue even after 8 h of irradiation with white LEDs, indicating persistence of S^{•+} in solution. By contrast, when the same polymerization was performed with LiBr present, the dark blue solution gradually turned light green (Figure S157), indicating a mixture of S^{•+} (blue) and S (yellow).

In an effort to improve polymerization control in a more challenging system, the synthesis of high-molecular-weight poly(methyl methacrylate) (PMMA) was undertaken.

Although high-molecular-weight polymers have been synthesized by a number of other controlled radical polymerization methods,^{40–45} they have remained elusive in O-ATRP. In part, this issue may be because the concentration of initiator must be reduced to target higher molecular weights, but the percentage of terminated chains in ATRP is predicted to vary inversely with the initiator concentration.⁴⁶ As such, to target higher-molecular-weight polymers, better deactivation may be necessary to control termination reactions.⁴⁷

To this end, a series of polymerizations were performed increasing the target molecular weight (M_{n,target}) of the polymer by varying the ratio of monomer to initiator. When these polymerizations were performed starting with S, polymers with low \bar{D} were consistently obtained, although I* increased undesirably over 100% with M_{n,target} (Table S12). Further, the number average molecular weight (M_n) measured for the polymers produced was limited to about 45 kDa, after which molecular weight growth began to plateau (Figures S158 and S163). We anticipated that performing these polymerizations using S^{•+} instead of S would improve these results, but no significant improvements were observed (Table S12). Even after varying the [LiBr] (Table S13) and S^{•+} loading (Table S14), the M_n of the product polymers remained limited to about 45 kDa. Further work is ongoing to determine the mechanistic cause of this limitation.

Polymerization of Acrylates. Another limitation of O-ATRP is its monomer scope, which remains narrow in comparison to traditional ATRP.¹² While different monomers present different challenges, acrylate monomers have been difficult to access in O-ATRP because of their large propagation rate constants. To compensate for an increase in the rate of propagation with acrylates relative to methacrylates, faster deactivation is necessary. Previously, our group reported two strategies to access the O-ATRP of acrylates. In the first, a new class of organic PCs, dihydroacridines, was developed, which featured strongly oxidizing radical cations to increase the thermodynamic

driving force for deactivation.²¹ More recently, a second strategy was reported, in which a dihydrophenazine PC was first reacted with diethyl 2-bromo-2-methylmalonate (DBMM) to generate a new substituted catalyst, followed by O-ATRP using this new PC. It was discovered that the reaction of the PC and DBMM not only led to the formation of a more oxidizing catalyst but also generated an excess of $\text{PC}^{\bullet+}$ prior to O-ATRP, which likely improved deactivation during the polymerization of acrylates.²⁰ In the present work, we hypothesized that the addition of isolated radical cations in the O-ATRP of acrylates would also improve polymerization control.

To first probe the impact of adding $\text{PC}^{\bullet+}$ to the polymerization of an acrylate (methyl acrylate, MA), a series of polymerizations were performed in which $[\text{S}^{\bullet+}]$ was increased while keeping the overall catalyst loading ($[\text{S}] + [\text{S}^{\bullet+}] = 100 \text{ ppm}$) constant (Table 2). With regard to the polymerization kinetics, increasing $[\text{S}^{\bullet+}]$ resulted in increasingly linear pseudo-first-order kinetics (Figure 9a) and a lower

$I^* = 86\%$ for $[\text{S}]:[\text{S}^{\bullet+}] = 0:1$). However, the most significant improvement was in the evolution of molecular weight during the polymerization, which decreased with only S , indicating no molecular weight control, but increased with $\text{S}^{\bullet+}$ (Figure 9b). Together, these results represent a significant improvement in the polymerization of MA using O-ATRP, although there are still several indicators of poor control in these results. For example, while \bar{D} was reduced through the use of $\text{S}^{\bullet+}$, a controlled polymerization should exhibit $\bar{D} \leq 1.5$. In addition, $I^* = 86\%$ for the O-ATRP of MA using $\text{S}^{\bullet+}$, but $I^* = 100\%$ is most desirable.

In an effort to further improve these results, an experiment was performed increasing $[\text{S}^{\bullet+}]$ along with $[\text{LiBr}]$ such that $[\text{LiBr}] = [\text{S}^{\bullet+}]$. Again, increasing the concentration of the radical cation resulted in a decrease in the rate of the polymerization (Figure 10), indicating improved deactivation

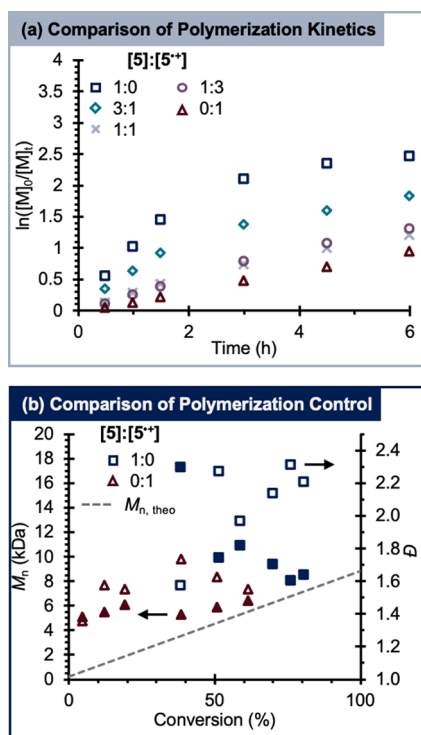


Figure 9. (a) Polymerization kinetics for the O-ATRP of MA catalyzed by S , demonstrating increasingly linear pseudo-first-order kinetics with increasing quantities of $\text{S}^{\bullet+}$. (b) Evolution of polymer molecular weight (M_n , filled shapes) and \bar{D} (hollow shapes) for the polymerization of MA by O-ATRP with S (blue) and $\text{S}^{\bullet+}$ (red).

rate of the polymerization ($k_{\text{obs}} = 0.89 \text{ M}^{-1} \text{ s}^{-1}$ for $[\text{S}]:[\text{S}^{\bullet+}] = 1:0$ vs $k_{\text{obs}} = 0.17 \text{ M}^{-1} \text{ s}^{-1}$ for $[\text{S}]:[\text{S}^{\bullet+}] = 0:1$). In particular, it is interesting that polymerizations with low $[\text{S}^{\bullet+}]$ exhibited downward sloping pseudo-first-order kinetics, as this feature is consistent with a prevalence of termination reactions due to poor deactivation.¹² The disappearance of this feature and the lowering of k_{obs} with increasing $[\text{S}^{\bullet+}]$ are consistent with improved deactivation.

Increasing $[\text{S}^{\bullet+}]$ also improved control during these polymerizations (Table 2). As $[\text{S}^{\bullet+}]$ increased, \bar{D} decreased ($\bar{D} = 1.77$ for $[\text{S}]:[\text{S}^{\bullet+}] = 1:0$ vs $\bar{D} = 1.55$ for $[\text{S}]:[\text{S}^{\bullet+}] = 0:1$) and I^* approached 100% ($I^* = 70\%$ for $[\text{S}]:[\text{S}^{\bullet+}] = 1:0$ vs I^*

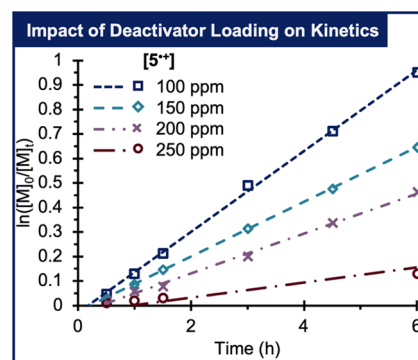


Figure 10. Polymerization kinetics for the O-ATRP of MA catalyzed by S , demonstrating a decrease in polymerization rate with increasing quantities of $\text{S}^{\bullet+}$.

with more $\text{S}^{\bullet+}$. In addition, improvements in polymerization control were observed up to 200 ppm $\text{S}^{\bullet+}$, resulting in $\bar{D} = 1.44$ and $I^* = 102\%$ (Table 3) vs $\bar{D} = 1.90$ and $I^* = 78\%$ with 200 ppm S and LiBr . Importantly, polymerizations performed by O-ATRP with 200 ppm S remained completely uncontrolled (Figure S172), indicating that these improvements are directly attributable to the presence of $\text{PC}^{\bullet+}$.

Unfortunately, further increasing $[\text{S}^{\bullet+}]$ above 200 ppm did not provide better control in the polymerization of MA; instead, it decreased control (Table 3, entry 16). We hypothesized that this decrease in control might be due to a background polymerization of MA, which is insignificant over shorter reaction times (6–14 h) but becomes competitive at longer reaction times (24 h). Control reactions support this hypothesis. When both $\text{S}^{\bullet+}$ and LiBr were removed (Table S15, entry S22), significant conversion of the monomer to polymer was still observed (57.1% at 14 h), and a high-molecular-weight polymer was recovered ($M_n = 467 \text{ kDa}$). Significant gelling of the reaction mixture was also observed (Figure S176), which is consistent with the free-radical polymerization of MA. For comparison, when the same control experiment was performed using MMA, only a 2% conversion and no gelling of the reaction mixture were observed.

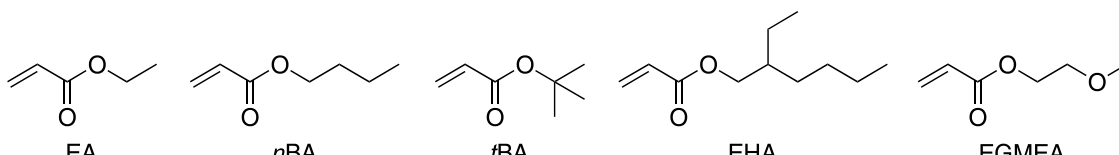
To balance improvements in polymerization control but suppress this background reaction, all remaining acrylate polymerizations were performed using 200 ppm $\text{S}^{\bullet+}$. Under these conditions, reaction variables were tuned in an effort to further improve polymerization control. For example, the

Table 3. Polymerization Results for the O-ATRP of MA with Increasing Quantities of 5^{++} ^a

entry	[5^{++}] (ppm)	time (h)	conv. (%) ^b	k_{obs} ($\text{M}^{-1} \text{h}^{-1}$) ^c	$M_{n,\text{theo}}$ (kDa)	$M_{n,\text{exp}}$ (kDa) ^d	\bar{D} ^d	I^* (%) ^e
13	100	6	61.4	0.16	5.54	6.45	1.55	86
14	150	10	69.3	0.11	6.22	6.97	1.44	89
15	200	14	71.3	0.08	6.39	6.25	1.44	102
16	250	24	53.5	0.02	4.86	4.26	1.83	114

^aFor all polymerizations, $[\text{MMA}]/[\text{DBMM}] = [1000]:[10]$ and $[\text{LiBr}] = [5^{++}]$ (see Section S12 of the Supporting Information for full experimental details). ^bDetermined by ^1H NMR. ^cDetermined from the first 6 h. ^dDetermined by GPC. ^eInitiator efficiency (I^*) = $(M_{n,\text{theo}}/M_{n,\text{exp}}) \times 100\%$.

Table 4. Results from the Polymerization of Various Acrylate Monomers by O-ATRP Using 5^{++} ^a

								
entry	monomer	time (h)	conv. (%) ^b	$M_{n,\text{theo}}$ (kDa)	$M_{n,\text{exp}}$ (kDa) ^c	\bar{D} ^c	I^* (%) ^d	
17	EA	14	64.2	6.68	6.72	1.47	99	
18	nBA	14	64.4	8.51	8.89	1.47	96	
19	tBA	14	84.1	11.0	9.36	1.74	118	
20	EHA	14	87.1	16.3	17.6	1.85	93	
21	EGMEA	14	87.0	11.6	13.5	1.60	86	

^aIn all cases, $[\text{monomer}]/[\text{DBMM}]/[5^{++}]/[\text{LiBr}] = [1000]:[10]:[0.2]:[0.2]$ (see Section S12 of the Supporting Information for full experimental details). ^bDetermined by ^1H NMR. ^cDetermined by GPC. ^dInitiator efficiency (I^*) = $(M_{n,\text{theo}}/M_{n,\text{exp}}) \times 100\%$.

choice of the solvent can have significant effects in O-ATRP,^{20,30,48} presumably by impacting the photophysics of the PC and ion pairing in $\text{PC}^{++}\text{Br}^-$. However, no improvements in O-ATRP using 5^{++} were obtained by changing the solvent. Using THF, similar results were obtained as with ethyl acetate (Table S16). By contrast, using DMAc led to a complete loss of control (Table S16, entry S31), likely because 5^{++} reacts with DMAc and decomposes to **5**. As a result, polymerizations in this solvent are more analogous to traditional O-ATRP using **5**.

In addition, the quantity of LiBr was varied while maintaining a constant $[5^{++}]$. We hypothesized that increasing $[\text{LiBr}]$ would improve polymerization control by further encouraging deactivation. However, it is also possible that adding more LiBr to the polymerization might increase the rate of the side reaction between 5^{++} and Br^- , leading to faster decomposition of 5^{++} to **5**. In this case, decreasing $[\text{LiBr}]$ might be more advantageous, as it might increase the lifetime of 5^{++} and improve deactivation during later reaction times. To test these hypotheses, polymerizations were performed varying the ratio of $[5^{++}]/[\text{LiBr}]$ from $[1]:[0.1]$ to $[1]:[10]$ (Table S17), but no improvements in polymerization control were observed.

We next sought to understand whether 5^{++} could be applied to the O-ATRP of other acrylate monomers. In total, five other acrylates were polymerized in this manner (Table 4). For monomers with shorter alkyl chains, ethyl acrylate (EA) and *n*-butyl acrylate (nBA), similar polymerization results were obtained as with MA. However, increasing the length of the alkyl chain led to a decrease in polymerization control (entry 20). In part, this observation can be attributed to the increase in the rate of propagation of acrylate monomers with longer alkyl chains.⁴⁹ In addition, increasing the length of the monomer alkyl substituent likely lowers the overall polarity of the polymerization solution, which might impact PC photo-physics and ion pairing in $\text{PC}^{++}\text{Br}^-$.

Finally, one important feature of all ATRP methods is the retention of the C–Br bonds at the ends of the polymer chains. This feature, termed chain-end group fidelity, is key for subsequent functionalization of the polymers produced by ATRP, such as by chain extension or block copolymer synthesis. As such, the chain-end fidelity of poly(methyl acrylate) (pMA) synthesized using 5^{++} was characterized and compared to pMA synthesized with **5**. We anticipated that the use of 5^{++} would yield superior chain-end fidelity since improving deactivation suppresses the termination reactions that cause loss of the Br functionality.

To investigate this property, we first synthesized pMA under optimized conditions using both **5** and 5^{++} (Table S18). The resulting polymers were characterized by ^1H NMR (Figures S188 and S189), which was consistent with the expected spectrum for pMA. To identify the chain ends arising from each set of polymerization conditions, the polymers were characterized by matrix-assisted laser desorption/ionization time-of-flight mass spectrometry (MALDI-TOF MS). For pMA synthesized using **5**, two peak distributions were observed, corresponding to two sets of end groups. The first distribution corresponded to polymers capped by the DBMM-derived malonate moiety and a Br end group. Instead, the second set of peaks was consistent with polymers containing the same malonate group and a H end group. Together, these results indicate that while some of the Br chain-end groups are retained, some loss of the Br functionality is also present. For pMA synthesized with 5^{++} , two distinct peak distributions were also observed. One set corresponded to the DBMM-derived malonate group on one end and Br on the other, the expected end groups. The other peak distribution corresponded to H and Br end groups, which can be explained by the proposed background polymerization, a free-radical polymerization that is ultimately suppressed by deactivation. Alternatively, the same end groups

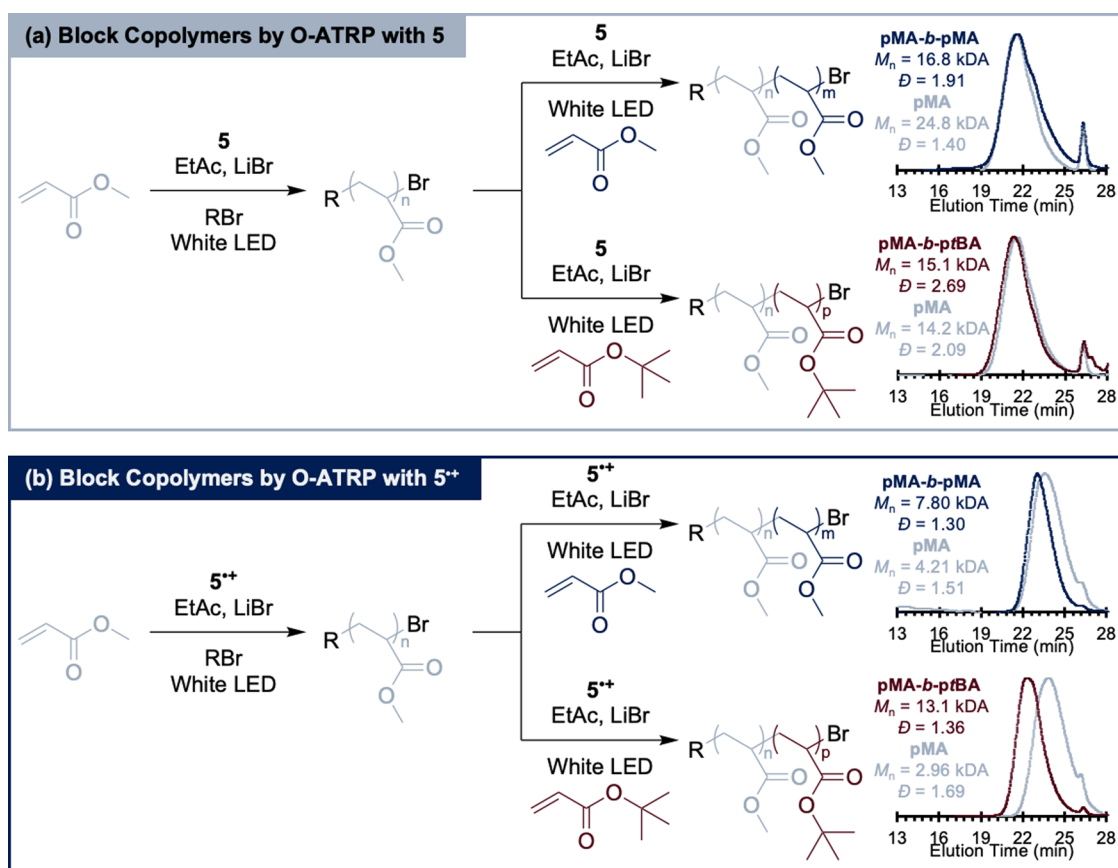


Figure 11. Synthesis of acrylate block copolymers by O-ATRP with **5** (a) and **5**** (b). GPC traces correspond to isolated and dried polymers as measured using a differential refractive index detector (see Section S12 of the [Supporting Information](#) for full experimental details).

could also arise from polymers initiated by Br^\bullet that ultimately undergo irreversible termination.

To further investigate chain-end fidelity in the absence and presence of 5^{**} , the synthesis of block copolymers was attempted using previously isolated pMA as a macroinitiator in place of DBMM. When pMA synthesized using **5** was resubjected to polymerization conditions in the presence of MA, the resulting polymer was nearly identical to the pMA macroinitiator (Figure 11a, blue). Similarly, when MA was replaced by *tert*-butyl acrylate (tBA), only a minor shift in the chromatogram of the block copolymer was observed relative to the macroinitiator (Figure 11a, red). These results indicate a significant loss of the Br chain ends during the O-ATRP of MA.

By contrast, when pMA synthesized with 5^{**} was resubjected to polymerization conditions in the presence of MA and tBA, clear evidence was found supporting the chain extension of this macroinitiator. In the case of pMA-*block*-pMA, a small shift in the chromatogram was observed (Figure 11b, blue) and the polymer molecular weight ($M_n = 7.80$ kDa) increased relative to the macroinitiator ($M_n = 4.21$ kDa). For pMA-*b*-ptBA, a more significant shift in the chromatogram (Figure 11b, red) and an increase in the copolymer molecular weight ($M_n = 13.1$ vs 2.96 kDa for pMA) were observed, providing evidence for improved chain-end fidelity for the polymerization using 5^{**} .

CONCLUSIONS

Radical cations of O-ATRP catalysts were synthesized and characterized by a combination of spectroscopic, electro-

chemical, and X-ray diffraction techniques. To understand their role and possible side reactions in O-ATRP, the reactivity of these compounds was investigated in solution, in deactivation model reactions, and in O-ATRP. Under the appropriate conditions, we discovered that these compounds can exhibit reactivity from both the ground state and a photoexcited state. However, the mechanism of this excited-state reactivity remains unclear, and deeper investigation of radical cation photophysics is necessary to understand this interesting phenomenon.

Using a deactivation model reaction, the ability of one PC^{**} to deactivate alkyl radicals was demonstrated by identification of the expected deactivation product. This model reaction was further used to investigate the impact of various factors on deactivation kinetics, such as the identity of the halide or the structure of PC^{**} . Ultimately, four main conclusions were drawn from these experiments: (1) $PC^{**}Br^-$ is likely the deactivator in O-ATRP; (2) the mechanism of deactivation appears to be concerted, where $PC^{**}Br^-$ undergoes a bimolecular reaction with the propagating radical; (3) deactivation with Br^- is faster than with Cl^- , likely because Cl^- is more challenging to oxidize; and (4) the oxidation potential of PC^{**} correlates with the rate of deactivation, such that more oxidizing radical cations exhibit faster deactivation.

When ion pairing in $PC^{**}PF_6^-$ was investigated by conductometry, the structure of PC^{**} was found to have only a minor impact on the strength of ion pairing. However, the polarity of the solvent significantly influences ion pairing, supporting the importance of solvent choice in O-ATRP.

Finally, the impact of radical cations on polymerization control in O-ATRP was investigated with two different monomers. While only limited improvements in polymerization control were observed with MMA, presumably because this system is already well controlled in the absence of added PC^{*+} , significant improvements in the polymerization of MA were achieved by performing O-ATRP with PC^{*+} instead of PC. Ultimately, this work demonstrates the importance of radical cations for deactivation in O-ATRP and shows how limitations in this polymerization method can be overcome by understanding their reactivity.

■ ASSOCIATED CONTENT

Supporting Information

The Supporting Information is available free of charge at <https://pubs.acs.org/doi/10.1021/acs.macromol.1c00640>.

Materials and methods; procedures; characterization of photocatalysts and radical cations; radical cation stability studies; investigation of radical cation excited-state reactivity; radical cation reactivity toward halides; deactivation of alkyl radicals by radical cations; investigation of hydrogen atom abstraction side reactions; ion pairing in radical cation hexafluorophosphate salts; general polymerization procedures; supplemental data for the polymerization of methyl methacrylate and methyl acrylate; and molecular coordinates for substrate oxidation calculations (PDF)

Crystallographic data file of 4^{*+}SbCl_6^- (CIF)

Crystallographic data file of 9^{*+}SbCl_6^- (CIF)

■ AUTHOR INFORMATION

Corresponding Author

Garret M. Miyake – Department of Chemistry, Colorado State University, Fort Collins, Colorado 80523-1872, United States; orcid.org/0000-0003-2451-7090;
Email: garret.miyake@colostate.edu

Authors

Daniel A. Corbin – Department of Chemistry, Colorado State University, Fort Collins, Colorado 80523-1872, United States

Blaine G. McCarthy – Department of Chemistry, Colorado State University, Fort Collins, Colorado 80523-1872, United States

Zach van de Lindt – Department of Chemistry, Colorado State University, Fort Collins, Colorado 80523-1872, United States

Complete contact information is available at:

<https://pubs.acs.org/doi/10.1021/acs.macromol.1c00640>

Notes

The authors declare no competing financial interest.

■ ACKNOWLEDGMENTS

Research reported in this publication was supported by the National Institute of General Medical Sciences (Award R35GM119702) of the National Institutes of Health. The content is solely the responsibility of the authors and does not necessarily represent the official views of the National Institutes of Health. The authors are grateful for support provided by Colorado State University and the Research Corporation for Science Advancement (Cottrell Scholar

Award). B.G.M. acknowledges support from the NSF GRFP. D.A.C. would like to thank Dr. Scott Folkman for helpful discussions of electrochemistry; Dr. Brian Newell, Cassidy Jackson, and Anthony Campanella for assistance with crystallography; and Cassidy Jackson for support throughout this work.

■ REFERENCES

- (1) Flory, P. J. Molecular size distribution in ethylene oxide polymers. *J. Am. Chem. Soc.* **1940**, *62*, 1561–1565.
- (2) Szwarc, M. Living polymers. *Nature* **1956**, *178*, 1168–1169.
- (3) Matyjaszewski, K.; Muller, A. H. E. 50 Years of living polymerization. *Prog. Polym. Sci.* **2006**, *31*, 1039–1040.
- (4) Grubbs, R. B.; Grubbs, R. H. 50th Anniversary perspective: living polymerization-emphasizing the molecule in macromolecules. *Macromolecules* **2017**, *50*, 6979–6997.
- (5) Hawker, C. J.; Wooley, K. L. The convergence of synthetic organic and polymer chemistries. *Science* **2005**, *309*, 1200–1205.
- (6) Kato, M.; Kamigaito, M.; Sawamoto, M.; Higashimura, T. Polymerization of methyl-methacrylate with the carbon-tetrachloride dichlorotris(triphenylphosphine)ruthenium(ii) methylaluminum bis-(2,6-di-tert-butylphenoxide) initiating system - possibility of living radical polymerization. *Macromolecules* **1995**, *28*, 1721–1723.
- (7) Wang, J. S.; Matyjaszewski, K. Controlled living radical polymerization - atom-transfer radical polymerization in the presence of transition-metal complexes. *J. Am. Chem. Soc.* **1995**, *117*, 5614–5615.
- (8) Solomon, D. H.; Rizzardo, E.; Cacioli, P. Polymerization Process and Polymers Produced Thereby. US4581429, July 11, 1984.
- (9) Chiefari, J.; Chong, Y. K.; Ercole, F.; Krstina, J.; Jeffery, J.; Le, T. P. T.; Mayadunne, R. T. A.; Meijs, G. F.; Moad, C. L.; Moad, G.; Rizzardo, E.; Thang, S. H. Living free-radical polymerization by reversible addition-fragmentation chain transfer: the RAFT process. *Macromolecules* **1998**, *31*, 5559–5562.
- (10) Miyake, G. M.; Theriot, J. C. Perylene as an organic photocatalyst for the radical polymerization of functionalized vinyl monomers through oxidative quenching with alkyl bromides and visible light. *Macromolecules* **2014**, *47*, 8255–8261.
- (11) Treat, N. J.; Sprafke, H.; Kramer, J. W.; Clark, P. G.; Barton, B. E.; de Alaniz, J. R.; Fors, B. P.; Hawker, C. J. Metal-free atom transfer radical polymerization. *J. Am. Chem. Soc.* **2014**, *136*, 16096–16101.
- (12) Kryszewski, P.; Matyjaszewski, K. Kinetics of atom transfer radical polymerization. *Eur. Polym. J.* **2017**, *89*, 482–523.
- (13) Matyjaszewski, K. Atom transfer radical polymerization (ATRP): current status and future perspectives. *Macromolecules* **2012**, *45*, 4015–4039.
- (14) Matyjaszewski, K. Advanced materials by atom transfer radical polymerization. *Adv. Mater.* **2018**, *30*, No. 1706441.
- (15) Pan, X. C.; Lamson, M.; Yan, J. J.; Matyjaszewski, K. Photoinduced metal-free atom transfer radical polymerization of acrylonitrile. *ACS Macro Lett.* **2015**, *4*, 192–196.
- (16) Theriot, J. C.; Lim, C. H.; Yang, H.; Ryan, M. D.; Musgrave, C. B.; Miyake, G. M. Organocatalyzed atom transfer radical polymerization driven by visible light. *Science* **2016**, *352*, 1082–1086.
- (17) Pearson, R. M.; Lim, C. H.; McCarthy, B. G.; Musgrave, C. B.; Miyake, G. M. Organocatalyzed atom transfer radical polymerization using N-aryl phenoxazines as photoredox catalysts. *J. Am. Chem. Soc.* **2016**, *138*, 11399–11407.
- (18) Chen, D. F.; Boyle, B. M.; McCarthy, B. G.; Lim, C. H.; Miyake, G. M. Controlling polymer composition in organocatalyzed photoredox radical ring-opening polymerization of vinylcyclopropanes. *J. Am. Chem. Soc.* **2019**, *141*, 13268–13277.
- (19) Su, X.; Jessop, P. G.; Cunningham, M. F. Versatility of organocatalyzed atom transfer radical polymerization and CO_2 -switching for preparing both hydrophobic and hydrophilic polymers with the recycling of a photocatalyst. *Macromolecules* **2019**, *52*, 6725–6733.

- (20) McCarthy, B.; Sartor, S.; Cole, J.; Damrauer, N.; Miyake, G. M. Solvent effects and side reactions in organocatalyzed atom transfer radical polymerization for enabling the controlled polymerization of acrylates catalyzed by diaryl dihydrophenazines. *Macromolecules* **2020**, *53*, 9208–9219.
- (21) Buss, B. L.; Lim, C.-H.; Miyake, G. M. Dimethyl dihydroacridines as photocatalysts in organocatalyzed atom transfer radical polymerization of acrylate monomers. *Angew. Chem., Int. Ed.* **2020**, *59*, 3209–3217.
- (22) Corbin, D. A.; McCarthy, B. G.; Miyake, G. M. Impacts of performing electrolysis during organocatalyzed atom transfer radical polymerization. *Polym. Chem.* **2020**, *11*, 4978–4985.
- (23) Jockusch, S.; Yagci, Y. The active role of excited states of phenothiazines in photoinduced metal free atom transfer radical polymerization: singlet or triplet excited states? *Polym. Chem.* **2016**, *7*, 6039–6043.
- (24) Koyama, D.; Dale, H. J. A.; Orr-Ewing, A. J. Ultrafast observation of a photoredox reaction mechanism: photoinitiation in organocatalyzed atom-transfer radical polymerization. *J. Am. Chem. Soc.* **2018**, *140*, 1285–1293.
- (25) Lewis-Borrell, L.; Sneha, M.; Bhattacharjee, A.; Clark, I. P.; Orr-Ewing, A. J. Mapping the multi-step mechanism of a photoredox catalyzed atom-transfer radical polymerization reaction by direct observation of the reactive intermediates. *Chem. Sci.* **2020**, *11*, 4475–4481.
- (26) Pan, X. C.; Fang, C.; Fantin, M.; Malhotra, N.; So, W. Y.; Peteanu, L. A.; Isse, A. A.; Gennaro, A.; Liu, P.; Matyjaszewski, K. Mechanism of photoinduced metal-free atom transfer radical polymerization: experimental and computational studies. *J. Am. Chem. Soc.* **2016**, *138*, 2411–2425.
- (27) Sartor, S. M.; McCarthy, B. G.; Pearson, R. M.; Miyake, G. M.; Damrauer, N. H. Exploiting charge-transfer states for maximizing intersystem crossing yields in organic photoredox catalysts. *J. Am. Chem. Soc.* **2018**, *140*, 4778–4781.
- (28) Sartor, S. M.; Lattke, Y. M.; McCarthy, B. G.; Miyake, G. M.; Damrauer, N. H. Effects of naphthyl connectivity on the photophysics of compact organic charge-transfer photoredox catalysts. *J. Phys. Chem. A* **2019**, *123*, 4727–4736.
- (29) Sartor, S. M.; Chrisman, C. H.; Pearson, R. M.; Miyake, G. M.; Damrauer, N. H. Designing high-triplet-yield phenothiazine donor-acceptor complexes for photoredox catalysis. *J. Phys. Chem. A* **2020**, *124*, 817–823.
- (30) Lim, C. H.; Ryan, M. D.; McCarthy, B. G.; Theriot, J. C.; Sartor, S. M.; Damrauer, N. H.; Musgrave, C. B.; Miyake, G. M. Intramolecular charge transfer and ion pairing in *N,N*-diaryl dihydrophenazine photoredox catalysts for efficient organocatalyzed atom transfer radical polymerization. *J. Am. Chem. Soc.* **2017**, *139*, 348–355.
- (31) Connelly, N. G.; Geiger, W. E. Chemical redox agents for organometallic chemistry. *Chem. Rev.* **1996**, *96*, 877–910.
- (32) Christensen, J. A.; Phelan, B. T.; Chaudhuri, S.; Acharya, A.; Batista, V. S.; Wasielewski, M. R. Phenothiazine radical cation excited states as super-oxidants for energy-demanding reactions. *J. Am. Chem. Soc.* **2018**, *140*, 5290–5299.
- (33) Parkin, G. Applications of deuterium isotope effects for probing aspects of reactions involving oxidative addition and reductive elimination of H-H and C-H bonds. *J. Labelled Compd. Radiopharm.* **2007**, *50*, 1088–1114.
- (34) Kolthoff, I. M.; Coetzee, J. F. Polarography in acetonitrile.2. Metal ions which have significantly different polarographic properties in acetonitrile and in water - anodic waves - voltammetry at rotated platinum electrode. *J. Am. Chem. Soc.* **1957**, *79*, 1852–1858.
- (35) Espenson, J. H. *Chemical Kinetics and Reaction Mechanisms*, 2nd ed.; McGraw-Hill: New York, NY, 2002.
- (36) Luo, Y.-R. *Comprehensive Handbook of Chemical Bond Energies*; CRC Press: Boca Raton, 2007.
- (37) Theriot, J. C.; McCarthy, B. G.; Lim, C. H.; Miyake, G. M. Organocatalyzed atom transfer radical polymerization: perspectives on catalyst design and performance. *Macromol. Rapid Commun.* **2017**, *38*, No. 1700040.
- (38) Fuoss, R. M. Ionic association.3. The equilibrium between ion pairs and free ions. *J. Am. Chem. Soc.* **1958**, *80*, 5059–5061.
- (39) Cole, J. P.; Federico, C. R.; Lim, C. H.; Miyake, G. M. Photoinduced organocatalyzed atom transfer radical polymerization using low ppm catalyst loading. *Macromolecules* **2019**, *52*, 747–754.
- (40) Carmean, R. N.; Becker, T. E.; Sims, M. B.; Sumerlin, B. S. Ultra-high molecular weights via aqueous reversible-deactivation radical polymerization. *Chem* **2017**, *2*, 93–101.
- (41) Xu, J. T.; Jung, K.; Atme, A.; Shanmugam, S.; Boyer, C. A robust and versatile photoinduced living polymerization of conjugated and unconjugated monomers and its oxygen tolerance. *J. Am. Chem. Soc.* **2014**, *136*, 5508–5519.
- (42) Gong, H. H.; Gu, Y.; Zhao, Y. C.; Quan, Q. Z.; Han, S. T.; Chen, M. Precise synthesis of ultra-high-molecular-weight fluoropolymers enabled by chain-transfer-agent differentiation under visible-light irradiation. *Angew. Chem., Int. Ed.* **2020**, *59*, 919–927.
- (43) Mueller, L.; Jakubowski, W.; Matyjaszewski, K.; Pietrasik, J.; Kwiatkowski, P.; Chaladaj, W.; Jurczak, J. Synthesis of high molecular weight polystyrene using AGET ATRP under high pressure. *Eur. Polym. J.* **2011**, *47*, 730–734.
- (44) Percec, V.; Guliasvili, T.; Ladislav, J. S.; Wistrand, A.; Stjern Dahl, A.; Sienkowska, M. J.; Monteiro, M. J.; Sahoo, S. Ultrafast synthesis of ultrahigh molar mass polymers by metal-catalyzed living radical polymerization of acrylates, methacrylates, and vinyl chloride mediated by SET at 25 degrees C. *J. Am. Chem. Soc.* **2006**, *128*, 14156–14165.
- (45) Rzaev, J.; Penelle, J. HP-RAFT: A free-radical polymerization technique for obtaining living polymers of ultrahigh molecular weights. *Angew. Chem., Int. Ed.* **2004**, *43*, 1691–1694.
- (46) Matyjaszewski, K. Comparison and Classification of Controlled/Living Radical Polymerizations. In *Controlled/Living Radical Polymerization: Progress in ATRP, NMP, and RAFT*; Matyjaszewski, K., Ed.; ACS Symposium Series; American Chemical Society, 2000; Vol. 768, pp 2–26.
- (47) Kwiatkowski, P.; Jurczak, J.; Pietrasik, J.; Jakubowski, W.; Mueller, L.; Matyjaszewski, K. High molecular weight polymethacrylates by AGET ATRP under high pressure. *Macromolecules* **2008**, *41*, 1067–1069.
- (48) Ryan, M. D.; Theriot, J. C.; Lim, C. H.; Yang, H. S.; Lockwood, A. G.; Garrison, N. G.; Lincoln, S. R.; Musgrave, C. B.; Miyake, G. M. Solvent effects on the intramolecular charge transfer character of *N,N*-diaryl dihydrophenazine catalysts for organocatalyzed atom transfer radical polymerization. *J. Polym. Sci., Part A: Polym. Chem.* **2017**, *55*, 3017–3027.
- (49) Beuermann, S.; Buback, M. Rate coefficients of free-radical polymerization deduced from pulsed laser experiments. *Prog. Polym. Sci.* **2002**, *27*, 191–254.